STATISTICAL ANALYSIS OF NETRAD HIGH RESOLUTION SEA CLUTTER

Riccardo Palamà, Maria Greco, Pietro Stinco, Fulvio Gini

Dipartimento di Ingegneria dell'Informazione, University of Pisa, Italy

ABSTRACT

This work deals with the analysis of spiky sea clutter data recorded by the high-resolution netted radar system NetRad, used in both the monostatic and bistatic configurations. The effects of spikes on the clutter statistics for monostatic radar signals have been widely studied, but for bistatic ones they are still under analysis. Statistically, the presence of spikes in the data is revealed by the long tails of the histograms, whose similarities with some theoretical models, such as the K, Weibull, Log-normal and the recently proposed Generalized Gaussian one, are examined in this paper. Particular attention is paid to the comparison between monostatic and bistatic data characteristics.

Index Terms— Bistatic radar, sea clutter, spikes, netted radar, Generalized Gaussian

1. INTRODUCTION

One of the hardest problems for the development and the performance evaluation of a maritime radar system is the presence of clutter, so the research on high resolution radar estimation and detection techniques cannot leave aside a detailed analysis of clutter properties. The radar sea clutter in the GHz range, at low grazing angle, and with a high range resolution is characterized by the presence of spikes, which are sequences of high-value samples, not expected in Gaussian process, lasting for up to some seconds. In particular, if a resolution cell contains a reduced number of scatterers, the Central Limit Theorem (CLT) does not apply and heavier tails are expected on the probability density function (PDF) of the In-phase (I) and Quadrature (Q) clutter components. In radar literature several studies [1],[2],[3],[4] have been done in order to model the clutter received by a monostatic system and some recent work [5] suggested the use of the Generalized Gaussian model. At the same time this analysis needs to be extended to the clutter collected by a bistatic radar system.

This work focuses on the statistical analysis of high resolution sea clutter data recorded by the NetRad system, a netted radar composed by a bistatic and a monostatic channel, working at both HH and VV polarization. After the necessary correction of the phase modulation introduced by the wireless synchronization system [6], we built the range-Doppler maps and we exploited them to locate the range interval where bistatic clutter power is mainly concentrated, that is, in the intersection of the bistatic receive and transmit antenna patterns. We compare the empirical distribution of the I and Q clutter samples with the Generalized Gaussian (GG) model, which belongs to the class of the Complex Elliptically Symmetric (CES) distributions [5], which includes also the very popular compound-Gaussian model [3], [7]. Furthermore the empirical distribution of the clutter amplitude is compared with some theoretical models, such as the Weibull, K [11], Lognormal and the GG, that is the PDF for the absolute value of a Generalized Gaussian random variable. In order to investigate the spikiness of the clutter, the information carried out by the kurtosis of the I-Q clutter components and by the Weibull shape parameter were examined, revealing some interesting properties of bistatic clutter, depending on the system polarization.

2. RADAR AND DATA DESCRIPTION

The analysis described in this paper is based on measured sea clutter data recorded by the NetRad system. The analyzed dataset was collected at Scarborough, Cape Town, in the Republic of South Africa on October 21, 2010. The radar was facing the Atlantic Ocean and was located on a bay. The NetRad system has been developed by the University College London (UCL), and can be used both in the monostatic and the bistatic configurations. A baseline of 728 m divides the two antennas, i.e. the monostatic and bistatic nodes, which are connected by a 5GHz wireless link. The carrier frequency is 2.4 GHz and the transmitted signal is an "up-down" chirp with a bandwidth of 45 MHz, which yields a 3.33 m range resolution (high range resolution).

For the analyzed dataset, in the bistatic configuration, the antennas of receiver (R) and transmitter (T) were pointed, in the azimuth direction, in order to create an isosceles triangle as shown in Fig.1. The clutter power is concentrated in the area illuminated by both antennas, within the range $[r_1, r_2]$, where:

$r_1 = 0.5L\cos(\theta/2)\cos^{-1}(\varphi - \theta/2)$, $r_2 = 0.5L\cos(\theta/2)\cos^{-1}(\varphi + \theta/2)$,

L is the baseline, while φ and θ denote respectively the azimuth pointing direction and the antenna azimuth half-power beamwidth that, for the analyzed system, is 11°, even though the antenna pattern is not ideal.

The measurements were made for different azimuth angles and for transmitted pulses of variable time duration,

while the elevation angle was fixed, equal to -1°. We analyzed many azimuth angles dataset but, for the lack of space, in this work we show only the results for $\varphi = 65°$. Each file dimension, after Hilbert filter decimation, is $N_p \times N_s$, where N_p, the number of pulse intervals (range cells), is $N_p=130000$, and N_s, the number of samples per sweep, is $N_s=1024$. The receiver chain, before the matched filter, included a Hamming windowing, mean-value subtraction and normalization of signals with respect to (wrt) the norm of the reference signal, i.e. the transmitted pulse [6].
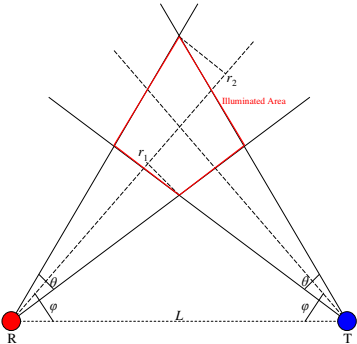
Fig. 1: Illuminated area for the bistatic configuration

3. SPECTRAL ANALYSIS AND PHASE CORRECTION

After the matched filter, periodograms were calculated for each range cell, as an estimate of the Power Spectral Density (PSD). The method adopted to compute periodograms was Welch's one, with a window of 256 samples and an overlap of 50% [8]. Finally, range-Doppler maps were plotted from the estimated PSDs. The range-Doppler maps of the bistatic channel show the effect of the phase deviation introduced by the synchronization system. In particular, the nodes are synchronized by a wireless link using two GPSDOs (GPS Disciplined Oscillators). Since these oscillators are independent, there is a difference between their oscillation frequencies, which causes a deviation of the relative phase between the signals from the bistatic and the monostatic nodes [6], [9]. This relative phase appears to be time-varying and generally non-linear. Due to this phase modulation, the clutter spectrum is spread out and its side-lobes raise, as can be noted in the range-Doppler maps of the bistatic data reported in Fig.2.

The spectrum of the direct signal, that is the signal received from the transmitter, can be observed in the zero-Doppler frequency bin with high side-lobes at other Doppler frequencies. Furthermore the spectrum of the clutter is contained within the illuminated interval $[r_1, r_2]$ on the range dimension, but it is spread on the frequency axis. In the following we will describe a phase correction technique to correct the effects introduced by the synchronization system.

The idea for the phase correction consists in using a fixed reference phase. This reference could be assumed by the phase of the received signal for the range cell which most probably contains a stationary target. Then the reference phase could represent the relative phase between the two nodes: for this reason it is subtracted from the phase of the received signal [9].
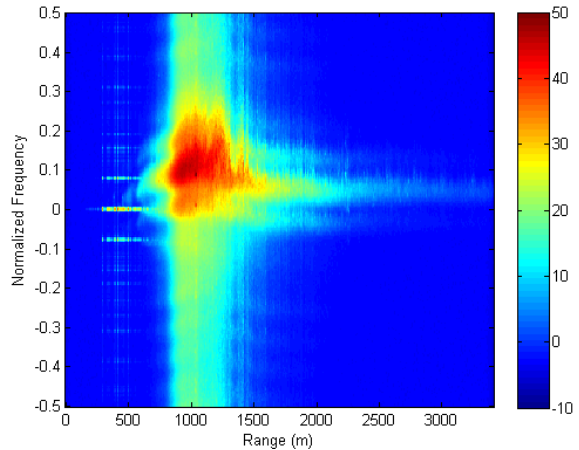
Fig. 2: Range-Doppler map, bistatic HH before phase correction, $\varphi=65°$

In order to apply this method, the position of the stationary target to be taken as reference has to be known. This obstacle may be bypassed by taking as a reference the phase of the direct signal, which is theoretically constant after the matched filter, except for a time-varying component, i.e. the phase term to be compensated. Anyway, selecting the range cell of the transmitter is not an automatic operation. Baseline amounts to 728 m, but figures show that the transmitter, i.e. the peak at zero-Doppler frequency, does not appear at this distance. Then phase correction may be performed by selecting as reference the range cell where the peak at zero-Doppler frequency is maximum.

Such an operation is carried out off-line by exploiting the signal at the output of the matched filter, since before this stage the phase for the range cell used as reference is very noisy. Furthermore the matched filter allows the received signal to be compressed in range dimension [9] . Denoting by $\mathbf{X}_l$ the vector containing the N_p I-Q range samples of the received signal corresponding to the l-th sweep pulse ($l=1, ... , N_S$), the phase correction is realized adjusting the phase of the received signal as [9]

$$\mathbf{X}_l^c = \mathbf{X}_l \cdot \exp\left(-j\boldsymbol{\theta}^{ref}\right) \ . \tag{1}$$

where $\boldsymbol{\theta}^{ref} = [\theta_1^{ref} \dots \theta_{N_p}^{ref}]^T$ in the N_px1 vector collecting the values of the reference phase.

Fig.3 shows the range-Doppler map of the phase-corrected signal. From this result it is easy to note that the bistatic clutter is contained within a well defined range interval, between 750 m and 1250 m, with the strongest peak in the range 850 m-1100 m.
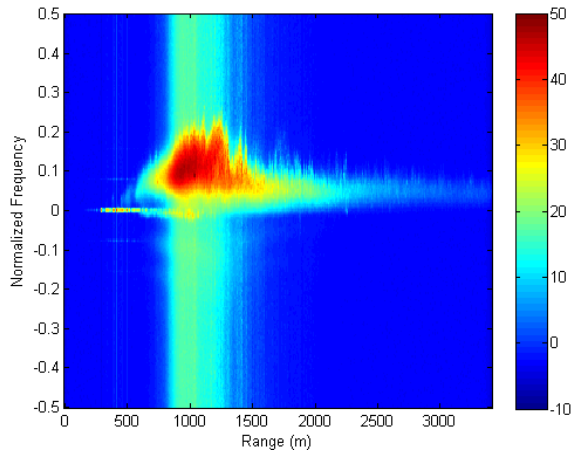
Fig. 3: Range-Doppler map, bistatic HH after phase correction, $\varphi=65°$

4. STATISTICAL ANALYSIS

After phase correction, the clutter data can be analyzed. The statistical analysis of clutter data was performed to evaluate the clutter properties with different azimuth angles and polarization. Furthermore, it was examined how clutter statistics change for a monostatic and bistatic radar system with high range resolution.

4.1. Analysis of IQ clutter components

Often, the complex envelope of the clutter $x=x_I+jx_Q$ is modeled as a complex Gaussian process, anyway, due to the spiky nature of clutter at high resolution and low grazing angles, the complex Gaussian model is not adequate. In the open literature, many heavy tailed distributions have been analyzed; in this work we show some results on the complex GG model [5]. The GG probability density function (PDF) is used to model the I and Q components of the clutter and it is given by:

$$f_x(x_I) = \frac{v}{2\alpha\Gamma(1/v)}\exp\left(-\left|\frac{x_I}{\alpha}\right|^v\right) \qquad (2)$$

where $\alpha > 0$ is the scale parameter, $v > 0$ is the shape parameter while $\Gamma(.)$ denotes the Gamma function. The Gaussian distribution is a special case of the GG, for shape parameter $v =2$ and scale parameter α equal to the standard deviation σ of the data. According to this consideration, large values of the scale parameter α are expected for range cells where clutter power is high.

The I and Q components of the collected sea-clutter data show a heavy-tailed histogram, which means a considerable number of spikes for both the HH and VV data. I-Q histograms appear to be very close to the GG model, which has a quite good fitting to the data also along tails of the PDF, as can be noted in Fig.4. For a deeper analysis of I and Q non Gaussianity, the kurtosis [10] was also evaluated,

since it measures the relative (w.r.t. the Gaussian one) peakeness or flatness of the distribution of IQ samples.
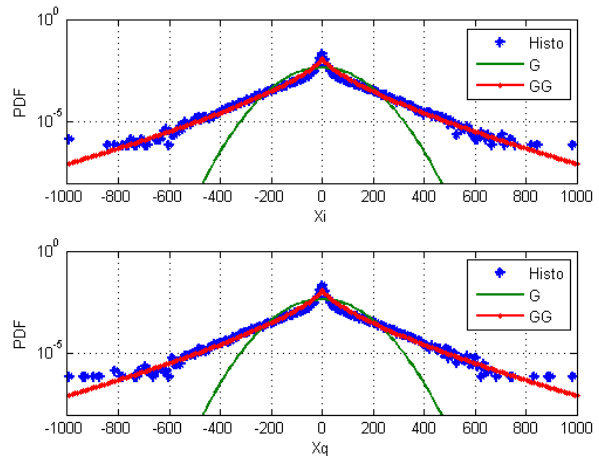
Fig. 4: Histograms of IQ clutter components, range=930m and azimuth $\varphi=65°$

For Gaussian data the kurtosis should be equal to 0. Kurtosis values of the I component are plotted as a function of the range in Fig. 5. Similar results have been obtained for the Q component, and are not reported here for lack of space.
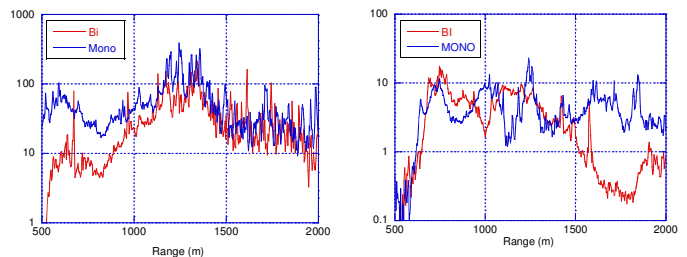
Fig. 5: In-Phase Kurtosis as a function of range $\varphi=65°$ (left HH, right VV)

As evident in Fig. 5, in the HH case, the kurtosis of the monostatic data is almost always (except really few samples) greater than that of the bistatic data, meaning that the monostatic data are spikier that the bistatic ones. This is not the case of the VV polarized data, for which, in many range cells in the area of maximum clutter power, the bistatic kurtosis is greater that the monostatic one, meaning that the spikiness of the bistatic clutter is not reduced wrt to that of the monostatic clutter. It is worth observing that, generally, HH data, both bistatic and monostatic, are spikier than VV data and this is confirmed by the different scales in left (1-1000) and right (0.1-100) plots in Fig. 5.

4.2. Analysis of Clutter Amplitudes

The analysis was completed by evaluating the distribution of the clutter amplitude, $r=|x|$, whose fitting with some theoretical distribution was examined. First, the distribution

of the amplitude of a complex GG r.v. was derived from [5], and it is given by

$$f_r\left(r;\beta,\alpha,b\right)=\frac{\beta}{\alpha\Gamma\left(\beta^{-1}\right)b^{1/\beta}}\,r\cdot\exp\left(-\frac{r^{2\beta}}{b\left(2\alpha\right)^{\beta}}\right)u\left(r\right) \qquad (3)$$

with shape parameter $\beta=v/2$ and $b=\left[\Gamma\left(\beta^{-1}\right)/\Gamma\left(2\beta^{-1}\right)\right]^{\beta}$. In addition, the n-order |GG| moment is given by

$$E\left\{r^{n}\right\}=\left(2\mu\right)^{n/2}b^{n/2\beta}\Gamma\left(\frac{n+1}{2\beta}\right)\Gamma^{-1}\left(\beta^{-1}\right). \qquad (4)$$

Similarly to the GG marginal PDF, the |GG| amplitude PDF collapses into a Rayleigh PDF if $\beta=1$. Our analysis was extended also to other theoretical distributions, such as the K, Weibull (W) and Log-normal (LN) distributions, which have been widely studied in radar literature in order to model sea clutter data recorded by high range resolution radar systems. The mathematical expressions of the theoretical PDFs and moments of the W, K and LN models can be found in [3].

The analysis of the empirical PDF of the clutter amplitude shows that clutter data exhibit different behavior depending on the examined range cell. For the bistatic channel, the HH polarized data from cells where clutter power is high seem to be appropriately represented by the K model, but the good fitting of this model gets less precise in the cells where clutter is less powerful. Such a behavior is not followed by the VV polarized data, which are less spiky than HH ones. In general, Weibull and |GG| models have a quite good fit with the data over the whole examined range (Fig. 6 and Fig. 7), especially where the power is high. The parameters of the theoretical distributions have been estimated using the Method of Moments (MoM) [3].

After an examination of the empirical PDFs of the data, our analysis was completed by evaluating the moments up to the 6-th order. The n-th order moment was normalized with respect to the n-th power of the mean value. These high-order statistics have shown a clutter behavior similar to that illustrated by the amplitude histograms, with the Weibull, the K and |GG| models best fitting the data, but for lack of space these results are not illustrated in this paper.

Because the Rayleigh distribution is a particular case of Weibull distribution of the shape parameter $c=2$, this shape parameter is often used as a measure of the spikiness of the clutter. The theoretical PDF of a Weibull r.v is as follows

$$f_{r,W}\left(r\right)=\frac{c}{b}\left(\frac{r}{b}\right)^{c-1}\exp\left[-\left(\frac{r}{b}\right)^{c}\right]u\left(r\right) \qquad (5)$$

Typically, the values of c span the interval [0.5-2]. The lower is c and the spikier is the clutter.
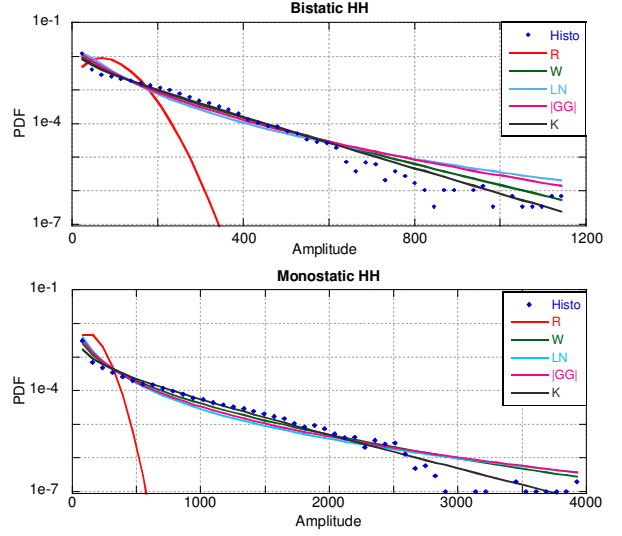
Fig. 6: Amplitude histograms of samples from a range cell of high clutter power, Range = 930 m, $\varphi=65°$, *HH pol*
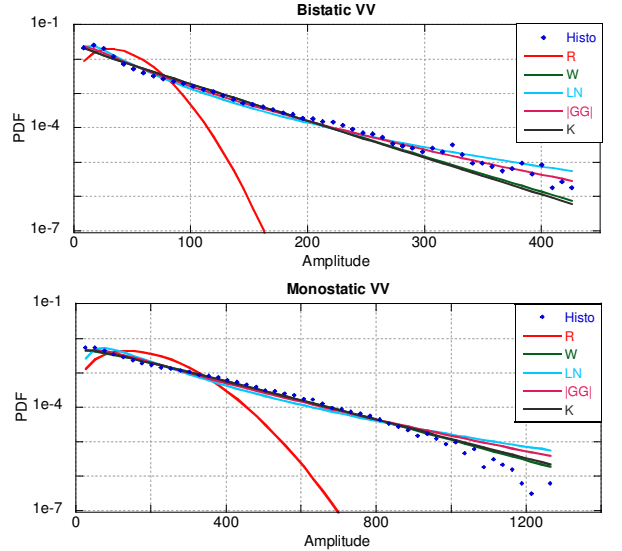
Fig. 7: Amplitude histograms of samples from a range cell of high clutter power, Range = 930 m, $\varphi=65°$, *VV pol*

Fig.8 shows the behavior of c vs the range for both HH (8a) and VV (8b) data, and it is easy to notice that the c parameter of bistatic HH data is always higher than that of monostatic data, but for VV data the behavior is different. There are many range cells where the bistatic c parameter is lower than the monostatic one, so confirming the results of the kurtosis in Fig.5. It is useful to observe that, after a distance of 1500m, the contribution of the noise for the bistatic data is not more negligible, since the overlap between transmit and receive antenna patterns is small and only on the side-lobes. That is why c, particularly for VV data, tends to 2.For a direct comparison between the values of c in bistatic and monostatic configurations, we report in Table I some values of the ratio of monostatic and bistatic c

(HH_m/HH_b and VV_m/VV_b) and of the ratio between HH and VV parameter c (HH_b/VV_b, HH_m/VV_m) for both configurations.
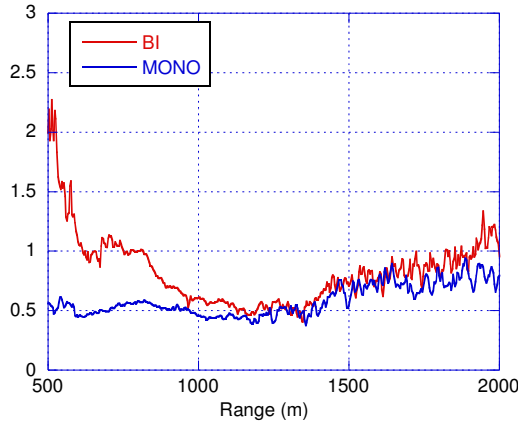
Fig. 8a: Weibull shape parameter as a function of range, HH data, $\varphi=65°$
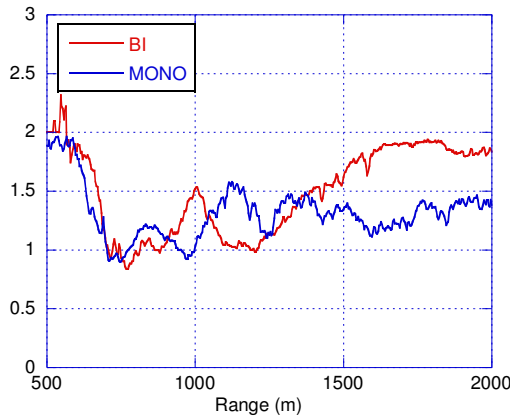
Fig. 8b: Weibull shape parameter as a function of range, VV data, $\varphi=65°$

Range (m)	HH_b/VV_b	HH_m/HH_b	HH_m/VV_m	VV_m/VV_b
810	1	0.56	0.50	1.13
850	0.83	0.65	0.46	1.16
890	0.69	0.74	0.46	1.11
930	0.70	0.79	0.51	0.95
1280	0.62	0.95	0.52	1.13
1430	0.71	0.87	0.39	0.82
1500	0.47	0.80	0.40	0.81

Tab. I: Ratios between c values for monostatic and bistatic configurations.

It can be easily observed that in monostatic configuration the HH data are much spikier than VV data ($HH_m/VV_m \simeq 0.48$). For bistatic data this ratio is close to 0.7. Moreover, passing from monostatic to bistatic configuration in HH pol. we have a reduction of spikiness

($HH_m/HH_b \simeq 0.7$), but in the VV pol. VV_m/VV_b is quite often greater than 1.

5. CONCLUSIONS

In this work we analyzed bistatic and monostatic sea clutter data recorded by the NetRad system with the aim of better characterizing the properties of bistatic clutter, especially its spikiness. The statistical analysis, carried on through histograms, moments and Weibull shape parameter analysis, has highlighted the differences between monostatic and bistatic clutter. Interestingly, we observed that in the bistatic case the spikiness of the HH data is greatly reduced with respect to the monostatic case, for the VV data unfortunately this is seldom true.

On going and future analysis will focus on statistical goodness-of-fit test, such as the modified Kolmogorov-Smirnov one [5], spectral analysis and dependency of the clutter characteristic on the bistatic angle.

REFERENCES

[1] J.B. Billingsley, A. Farina, F. Gini, M. Greco, L. Verrazzani, "Statistical analyses of measured radar ground clutter data", *IEEE Trans. on AES*, Vol. 35, No. 2, pp. 579-593, 1999.

[2] V. Anastassopoulos, G.A. Lampropoulos, A. Drosopoulos, M. Rey, "High resolution radar clutter statistics," *IEEE Trans. on AES*, vol.35, no.1, pp.43,60, Jan 1999.

[3] M. Greco, F. Gini, M. Rangaswamy, "Statistical analysis of real polarimetric clutter data at different range resolutions," *IEE Proc. Radar, Sonar and Navigation*, Vol. 153, No. 6, pp. 473-481, Dec. 2006.

[4] M. Greco, P. Stinco, F. Gini, "Identification and analysis of sea radar clutter spikes," *IET-RSN*, vol.4, no.2, pp.239-250, April 2010.

[5] E. Ollila, D.E. Tyler, V. Koivunen, H.V. Poor, "Complex Elliptically Symmetric Distributions: Survey, New Results and Applications," *IEEE Trans. on SP*, vol.60, no.11, pp.5597-5625, Nov. 2012.

[6] W.A.M. Al-Ashwal, *Measurement and Modelling of Bistatic Sea Clutter*, PhD thesis, University College London,2011.

[7] M. Greco, P. Stinco, F. Gini, M. Rangaswamy, "Impact of Sea Clutter Nonstationarity on Disturbance Covariance Matrix Estimation and CFAR Detector Performance,"*, IEEE Transactions on AES*, vol.46, no.3, pp.1502,1513, July 2010.

[8] P.D. Welch, "The use of fast Fourier transform for the estimation of power spectra: A method based on time averaging over short, modified periodograms"*, IEEE Trans. on Audio and Electroacoustics*, vol.15, no.2, pp.70,73, Jun 1967.

[9] J.S. Sandenbergh, M.R. Inggs, W.A.M Al-Ashwal, "Evaluation of coherent netted radar carrier stability while synchronised with GPS-disciplined oscillators," *2011 IEEE Radar Conference*, pp.1100-1105, May 2011.

[10] S. M. Kay, *Fundamentals of Statistical Signal Processing, Estimation Theory, Vol. I*, Prentice Hall PTR, Upper Saddle River, New Jersey 07458.

[11] M.A. Ritchie et al. "Coherent analysis of horizontally-polarized monostatic and bistatic sea clutter," *Radar Systems(Radar 2012), IET International Conference on* , vol., no., pp.1,5, 22-25 Oct. 2012